IOP PUBLISHING JOURNAL OF PHYSICS D: APPLIED PHYSICS

J. Phys. D: Appl. Phys. **46** (2013) 065502 (13pp) doi:10.1088/0022-3727/46/6/065502

Current flow in a 3-terminal thin film contact with dissimilar materials and general geometric aspect ratios

Peng Zhang, Derek M H Hung and Y Y Lau

Department of Nuclear Engineering and Radiological Sciences, University of Michigan, Ann Arbor, MI 48109-2104, USA

E-mail: yylau@umich.edu

Received 4 November 2012, in final form 14 December 2012
Published 17 January 2013
Online at stacks.iop.org/JPhysD/46/065502

Abstract

The current flow pattern, together with the contact resistance, is calculated analytically in a Cartesian 3-terminal thin film contact with dissimilar materials. The resistivities and the geometric dimensions in the individual contact members, as well as the terminal voltages, may assume arbitrary values. We show that the current flow patterns and the contact resistance may be conveniently decomposed into the even and odd solution. The even solution gives exclusively and totally the current flowing from the source to the gate. The odd solution gives exclusively and totally the current flowing from the source to the drain. Current crowding at the edges, and current partition in different regions are displayed. The analytic solutions are validated using a simulation code. The bounds on the variation of the contact resistance are given. This paper may be considered as the generalization of the transmission line model and the Kennedy–Murley model that were used extensively in the characterization of thin-film devices. For completeness, we include the general results for the cylindrical geometry, which are qualitatively similar to the even solution of the Cartesian geometry.

(Some figures may appear in colour only in the online journal)

1. Introduction

3-terminal thin-film contacts are ubiquitous to modern electronic devices. They are also used extensively in semiconductor material and device characterization [1]. Since their characteristics determine the device performances [1, 2], a systematic investigation of them would be of value. For example, in the miniaturization of electronics, the effects of current crowding and Joule heating become significant [3]. In superconducting nanocircuits, the current crowding effects at the 3-terminal structure are known to cause critical current reduction [4]. Thus, it is worthwhile to quantify, in detail, the current flow and contact resistance in 3-terminal thin film contacts. This paper provides such a study.

The most commonly used model for thin film contacts is the transmission line model (TLM), which was proposed by Berger [2, 5] and by Murrmann and Widmann [6] in the 1970s. In TLM, the 3-terminal thin film contact is approximated by a transmission line, assuming that the conducting thin film layer has a zero thickness. Kennedy and Murley [7] numerically calculated the current distribution and electrical resistance for a thin film contact, with the assumption of zero resistance for the contact layer. Here, we relax the assumptions adopted in the TLM model and in the Kennedy–Murley model through a field analysis of a 3-terminal thin film geometry with arbitrary aspect ratios and resistivity ratios (figure 1).

Motivated by the classical work on electrical contacts of Holm [8] and Timsit [9, 10], we recently developed analytical models to study both bulk contacts [11, 12][1] and thin film contacts [13–15], including the effects of higher dimensions and dissimilar materials. Simple, analytical scaling laws of contact resistance for both bulk and thin film contacts were proposed. The current crowding effect, which may induce excessive ohmic heating, was studied. Our dc thin film contact

[1] There was a typo in [12]. In equation (6) [12], the term $-2.2281(a/b)^2$ in $g(b/a)$ should read $-1.2281(a/b)^2$.

 © 2013 IOP Publishing Ltd Printed in the UK & the USA

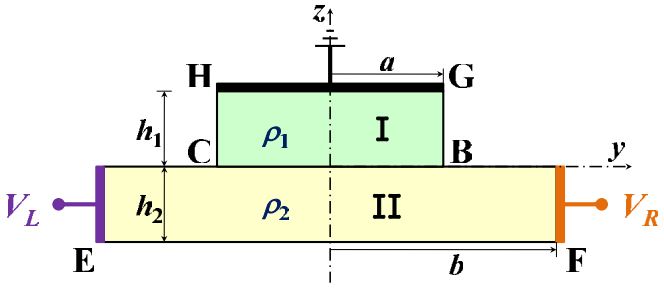

Figure 1. 3-terminal Cartesian thin film contact structure of dissimilar materials, with arbitrary terminal voltage at the three terminals. This figure may be considered as the superposition of figures 2 and 3.

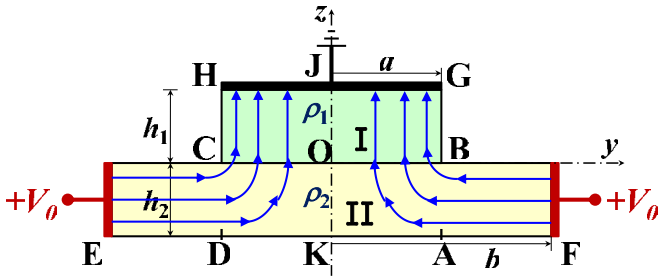

Figure 2. Even part of the 3-terminal Cartesian thin film contact in figure 1. This figure also represents the cylindrical geometry, where the z-axis is the axis of rotation.

resistance calculation is extended to a thin film contact of an arbitrary shape; it is also found to be applicable to ac bulk contact resistance calculations [15, 16]. While this recent analytic theory of Cartesian thin film contact is verified in various limits and simulations, it has two major restrictions: (1) the height of the top contact member, h_1 in figure 1, is assumed to be large compared with a, and (2) the left and right terminals (figure 1) take on the same voltage [13–16]. This paper relaxes these two assumptions.

The Cartesian thin film geometry is shown in figure 1. Without loss of generality, we assume that the top terminal GH is at zero potential. The left terminal E is at voltage $V_{\rm L}$ and the right terminal F is at voltage $V_{\rm R}$. Region I has electrical resistivity ρ_1, thickness h_1, and width $2a$, and region II has electrical resistivity ρ_2, thickness h_2, and width $2b$. All parameters ρ_1, ρ_2, h_1, h_2, a, b ($>a$), $V_{\rm L}$ and $V_{\rm R}$ may assume arbitrary values. The model in figure 1 may be decomposed into two parts, the even part and the odd part. In the even part, the voltages at both terminals E and F are held at the same voltage $+V_0$, as shown in figure 2, where all symbols are defined. In the odd part, the voltage at terminal E is held at the voltage $-V_0'$ and the voltage at terminal F is held at the opposite voltage $+V_0'$, as shown in figure 3. If we set $V_0 = (V_{\rm R}+V_{\rm L})/2$ and $V_0' = (V_{\rm R}-V_{\rm L})/2$, so that $V_0-V_0' = V_{\rm L}$, and $V_0 + V_0' = V_{\rm R}$, the potential and current flow solutions in figure 1 are, respectively, the sum of the potential and of current flow solutions in figures 2 and 3 from the superposition principle.

This decomposition into even and odd solution is physically significant. Let us call terminal F in figure 1 the 'source', terminal E the 'drain', and terminal GH the 'gate'. Then the even solution gives all of the current that is transported to the gate, as shown in figure 2. The odd solution gives all of the current that is transported to the drain, as shown in figure 3, because the *total* current that reaches the gate is zero. In figure 3, the current arriving at GJ is exactly cancelled by the current leaving JH, by symmetry, making the *total* current arriving at the gate GH equal to zero. Specifically, the total current that arrives at the gate of figures 1 and 2 is simply $I_{\rm gate} = V_0/R$, where R is given by equation (1) in which $\bar{R}_{\rm c}$(E) is the contact resistance for the even solution that is given by the exact expression equation (A7) and displayed graphically in figure 5. Similarly, the total current that arrives at the drain of figures 1 and 3 is simply $I_{\rm drain} = V_0'/R$, where R is given by equation (2) in which $\bar{R}_{\rm c}(O)$ is the contact resistance for the odd solution that is given by the exact expression (equation (B8)) and displayed graphically in figure 8. The total current that leaves the source is $I_{\rm source} = I_{\rm drain} + I_{\rm gate}$ by current conservation.

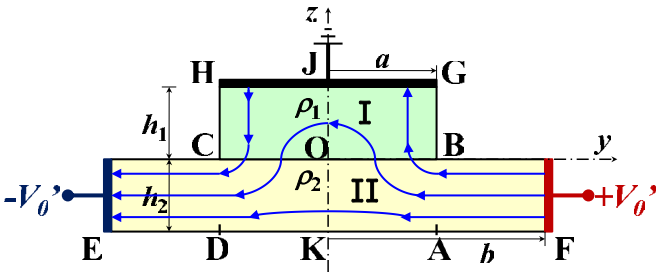

Figure 3. Odd part of the 3-terminal Cartesian thin film contact in figure 1.

From the exact expressions of the electrostatic potentials in regions I and II, we calculate the electric field pattern everywhere (see figure 6 for the even solution and figure 10 for the odd solution). For the odd solution (figure 3), the splitting of the current that is transported to JG, across JO and across OK is shown in figure 9. These quantities are not readily available in simulation codes such as MAXWELL [17][2]. Note that the odd solution gives all of the current transport across the mid-plane in figure 1 (represented by the z-axis), because the even solution does not provide such current transport (figure 2).

For completeness, we include the cylindrical geometry of figure 2 where the z-axis represents the axis of rotation, and terminals E and F represent the circular anode (rim) at voltage V_0. The top electrode HG is grounded; and all parameters ρ_1, ρ_2, h_1, h_2, a, b ($>a$) may assume arbitrary values. The current flow pattern for this cylindrical geometry is also given by figure 2 qualitatively.

In section 2, we consider the Cartesian thin film. Section 2.1 presents the even solution and section 2.2 presents the odd solution. For both solutions, we present the contact resistance, its validation using the MAXWELL 2D code [17], and its current pattern. In section 3, we consider the cylindrical thin film, which is qualitatively similar to the even solution of section 2.1. Concluding remarks are given in section 4, where we outline our further generalization to a Cartesian thin film geometry that is non-symmetrical about the z-axis in figure 1. Only the major results will be presented in the main text. Their

[2] For the present electrostatic problem, MAXWELL 2D uses automatic meshing and finite element analysis to solve the Laplace equation.

derivations, based on Fourier series analysis, are given in the appendices.

2. Cartesian thin film contact

We shall first make a few general remarks concerning the even and odd solutions shown in figures 2 and 3. (1) We used Fourier series to solve the Laplace equation in regions I and II, and match the boundary conditions at the interface. This technique was described in detail in our treatment of thin-film contacts [13] and in bulk contacts [12]. (2) If terminal E(F) is sufficiently far from point D(A), the current flow at E(F) is uniform and the contact or spreading resistance at the corner C(B) is independent of b. This condition is satisfied if either $b \gg h_2$ or $b \gg a$. (3) The limit, $\rho_1/\rho_2 \to 0$ at a fixed value of h_1/a, gives the same contact resistance as the limit, $h_1/a \to 0$ at a fixed value of ρ_1/ρ_2, because in either case, the ground at HG is effectively placed at the interface BC. (4) For the even case, figure 2, we have solved for the limit $h_1/a \gg 1$ in [13]. This paper extends [13] to arbitrary values of h_1/a. See also point (3). (5) The odd solution for figure 3 is new, because the boundary GJK is at zero potential in figure 3. Bearing these points in mind for an understanding of the data, we report the detailed results on the even and odd case in sections 2.1 and 2.2.

2.1. Even case

For the even case (figure 2), the geometry is symmetrical about the vertical z-axis. The potential profile within the structure is an even function of y. The current flow patterns (and the field lines) are symmetrical about the z-axis. All current flowing from terminals E and F ends up at the gate GH. The total current that reaches the gate is $I_{\text{gate}} = V_0/R$, where R is the resistance from terminals E and F to the gate GH and is found to be

$$R = \rho_2 \frac{b-a}{2h_2 \times W} + \frac{\rho_2}{4\pi W} \bar{R}_c(\text{E}) \left(\frac{a}{b}, \frac{h_1}{a}, \frac{a}{h_2}, \frac{\rho_1}{\rho_2} \right) + \rho_1 \frac{h_1}{2a \times W}, \quad (1)$$

where W denotes the channel width in the third, ignorable dimension that is perpendicular to the paper. In equation (1), the first term represents the bulk resistance of the thin film base, from A to F, and from D to E. The third term represents the bulk resistance of the top region from BC to GH. The second term represents the remaining constriction (or contact) resistance, R_c(E), for region ABCD, and is expressed as $R_c = (\rho_2/4\pi W)\bar{R}_c(\text{E})$ for the even case. The normalized $\bar{R}_c(\text{E})$ depends on the aspect ratios a/b, h_1/a, a/h_2, and on the resistivity ratio ρ_1/ρ_2, as explicitly shown in equation (1). The *exact* expression for $\bar{R}_c(\text{E})$ is derived in appendix A (see equation (A7)). In the following analysis, we assume either $b \gg a$ or $b \gg h_2$, in which case $\bar{R}_c(\text{E})$ is independent of b [13]. This condition is easily satisfied according to the flow patterns shown in figures 6 and 10. See also comment (2) in the first paragraph of this section.

In the limit $h_1/a \to \infty$, $\bar{R}_c(\text{E})$ was studied in detail in [13], and its value as a function of a/h_2 at various values of ρ_1/ρ_2 is shown in figure 4. The solid lines in figure 4 show

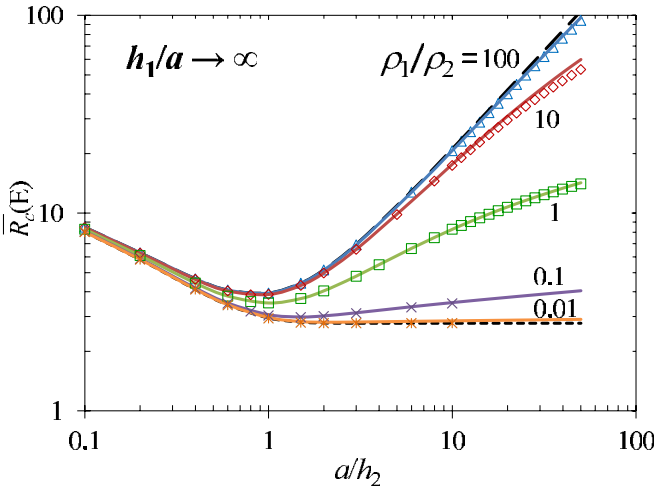

Figure 4. $\bar{R}_c(E)$ in the limit of $h_1/a \to \infty$, for the even solution of Cartesian thin film contact (figure 2). The solid lines represent the synthesized scaling law (equation (A8)), symbols represent the exact calculations (equation (A7)), and the upper and lower dashed lines represent the limiting cases, respectively, of $\rho_1/\rho_2 \to \infty$ (equation (A13)), and of $\rho_1/\rho_2 \to 0$ (equation (A11)).

the new fitting formula, equation (A8) of appendix A, which is more elegant and more accurate than the fitting formula that was published in [13]. In the opposite limit $h_1/a \to 0$, $\bar{R}_c$(E) is given by equation (A15). These two equations, equations (A8) and (A15), define the bounds on each sub-figure in figure 5.

Figure 5 shows the exact theory for $\bar{R}_c$(E) (see equation (A7)) as a function of a/h_2, for various ρ_1/ρ_2, addressing the effect of h_1/a in each sub-figure. For a given resistivity ratio ρ_1/ρ_2, $\bar{R}_c$(E) increases as h_1/a increases at fixed a/h_2. The range of $\bar{R}_c$(E) increases as a/h_2 increases. For each sub-figure of a given ρ_1/ρ_2 in figure 5, the bounds of the curves are governed by equations (A8) and (A15), as mentioned in the preceding paragraph. If ρ_1/ρ_2 is small, as in figure 5(a) for $\rho_1/\rho_2 = 0.01$, h_1/a has little effect on $\bar{R}_c$(E). As ρ_1/ρ_2 increases, the effect h_1/a on $\bar{R}_c$(E) is more pronounced. The analytic theory is verified by MAXWELL 2D simulation results [17], represented by the symbols in figure 5.

The field line equation, $y = y(z)$, may be numerically integrated from the first-order ordinary differential equation $\mathrm{d}y/\mathrm{d}z = E_y/E_z = (\partial\Phi/\partial y)/(\partial\Phi/\partial z)$ where Φ is given by equation (A1). The field lines in the right half of the thin film structure (figure 2) are shown for the special cases of $\rho_1/\rho_2 = 1$ and $h_1/a = 0.01$ with various a/h_2 in figures 6(a)–(c); $\rho_1/\rho_2 = 1$ and $a/h_2 = 5$ with various h_1/a in figures 6(d)–(f); and $h_1/a = 0.1$ and $a/h_2 = 5$ with various ρ_1/ρ_2 in figures 6(g)–(i). It is clear that as a/h_2 increases, the field lines (also the current flow lines) are more crowded towards the constriction corner B, as shown in figures 6(a)–(c), indicating more enhanced local heating there. As h_1/a increases, the field lines across the interface BC become more uniformly distributed, as shown in figures 6(d)–(f). As ρ_1/ρ_2 increases in figures 6(g)–(i), the field lines become more uniformly distributed, because the boundary BC becomes increasingly like an equipotential with respect to region I.

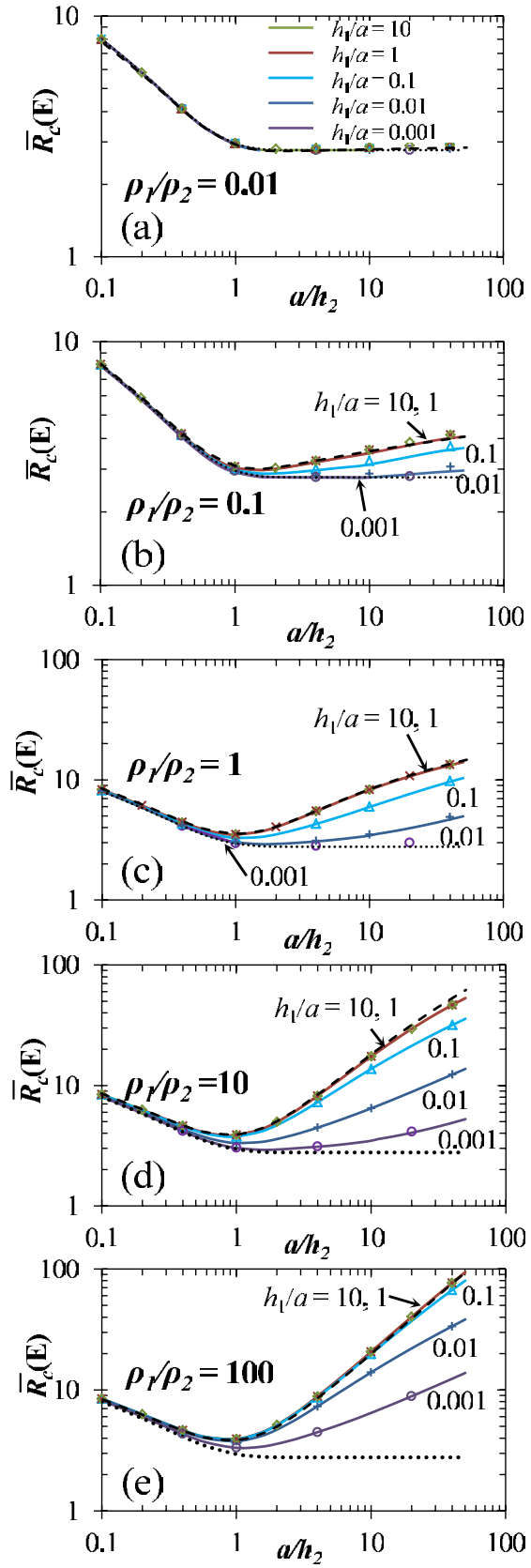

Figure 5. $\bar{R}_c(E)$ as a function of a/h_2, for $\rho_1/\rho_2 = 0.01$ (*a*), 0.1 (*b*), 1 (*c*), 10 (*d*), and 100 (*e*), with the effect of h_1/a displayed in each sub-figure. The solid lines represent the exact calculations (equation (A7)), symbols represent MAXWELL 2D simulation, the dashed lines represent equation (A8) and the dotted lines represent equation (A15).

2.2. *Odd case*

For the odd case (figure 3), the geometry is also symmetrical about the vertical z-axis. The potential profile is an odd function of y. Thus, the entire boundary GJK is at zero potential. All current flows from terminal F ends up at terminal E, the drain, because there is no net current that flows into the gate GH in figure 3. The total current that reaches the drain (terminal E) is the same as the current that intercepts the boundary GJK. It is therefore given by $I_{\text{drain}} = V_0'/R$, where R is given by

$$R = \rho_2 \frac{b-a}{h_2 \times W} + \frac{\rho_2}{4\pi W} \bar{R}_c\,(\mathrm{O}) \left(\frac{a}{b}, \frac{h_1}{a}, \frac{a}{h_2}, \frac{\rho_1}{\rho_2} \right), \qquad (2)$$

where W denotes the channel width in the third, ignorable dimension that is perpendicular to the paper, and the rest of the symbols have been defined in figure 3. In equation (2), the first term represents the bulk resistance of the thin film base, from A to F. The second term represents the remaining constriction (or contact) resistance, $R_c(\mathrm{O})$, for region AGJK. The constriction (contact) resistance is normalized in the form as $R_c(\mathrm{O}) = (\rho_2/4\pi W)\bar{R}_c(\mathrm{O})$, where $\bar{R}_c(\mathrm{O})$ depends on the aspect ratios $a/b, h_1/a, a/h_2$, and on the resistivity ratio ρ_1/ρ_2, as explicitly shown in equation (2). The *exact* expression for $\bar{R}_c(\mathrm{O})$ is derived in appendix B (see equation (B8)). In the following analysis, we assume $b \gg a$ or $b \gg h_2$, in which case $\bar{R}_c(\mathrm{O})$ is independent of b [13], as in the even case.

We first consider the limiting case of $h_1/a \to \infty$. In figure 7, the exact theory of $\bar{R}_c(\mathrm{O})$ (see equation (B8)) is plotted as a function of a/h_2, for various ρ_1/ρ_2, in this limit. In general, $\bar{R}_c(\mathrm{O})$ increases as a/h_2 increases. For a given a/h_2, $\bar{R}_c(\mathrm{O})$ increases as ρ_1/ρ_2 increases. The range of variation $\bar{R}_c(\mathrm{O})$ increases as a/h_2 increases. In the limit of $\rho_1/\rho_2 \to \infty$, region BCHG (figure 3) acts as an insulator with respect to the base region BCEF, current flows directly from right to left, and it is easy to show that

$$\bar{R}_c(\mathrm{O})|_{\rho_1/\rho_2 \to \infty} = 4\pi \frac{a}{h_2}, \qquad (3)$$

which is also plotted as the top dashed curve in figure 7. Note that the exact theory for $\rho_1/\rho_2 = 100$ overlaps with equation (3). In the opposite limit, $\rho_1/\rho_2 \to 0$, region BCHG (figure 3) acts as a perfectly conducting material with respect to the base region BCEF. Thus, the whole constriction interface BC is an equipotential surface, as if $h_1 = 0$ and the top electrode is applied directly to the interface BC for the Cartesian geometry. This special case is analysed by Hall using conformal mapping (see figure 35 and equation (52) of Hall's 1967 paper [18]), and from which $\bar{R}_c(\mathrm{O})$ in the limit of $\rho_1/\rho_2 \to 0$ is given as

$$\bar{R}_c(\mathrm{O})|_{\rho_1/\rho_2 \to 0} = 4\pi \frac{a}{h_2} - 8 \ln \left[\cosh \left(\frac{\pi}{2} \frac{a}{h_2} \right) \right], \qquad (4)$$

which is plotted as the bottom dashed curve in figure 7. Note that the exact theory for $\rho_1/\rho_2 = 0.01$ overlaps with equation (4). In the limit of $\rho_1/\rho_2 \to 0$, $\bar{R}_c(\mathrm{O})$ converges to a constant value of $8 \ln 2 = 5.55$ for $a/h_2 > 2$, as shown in figure 7.

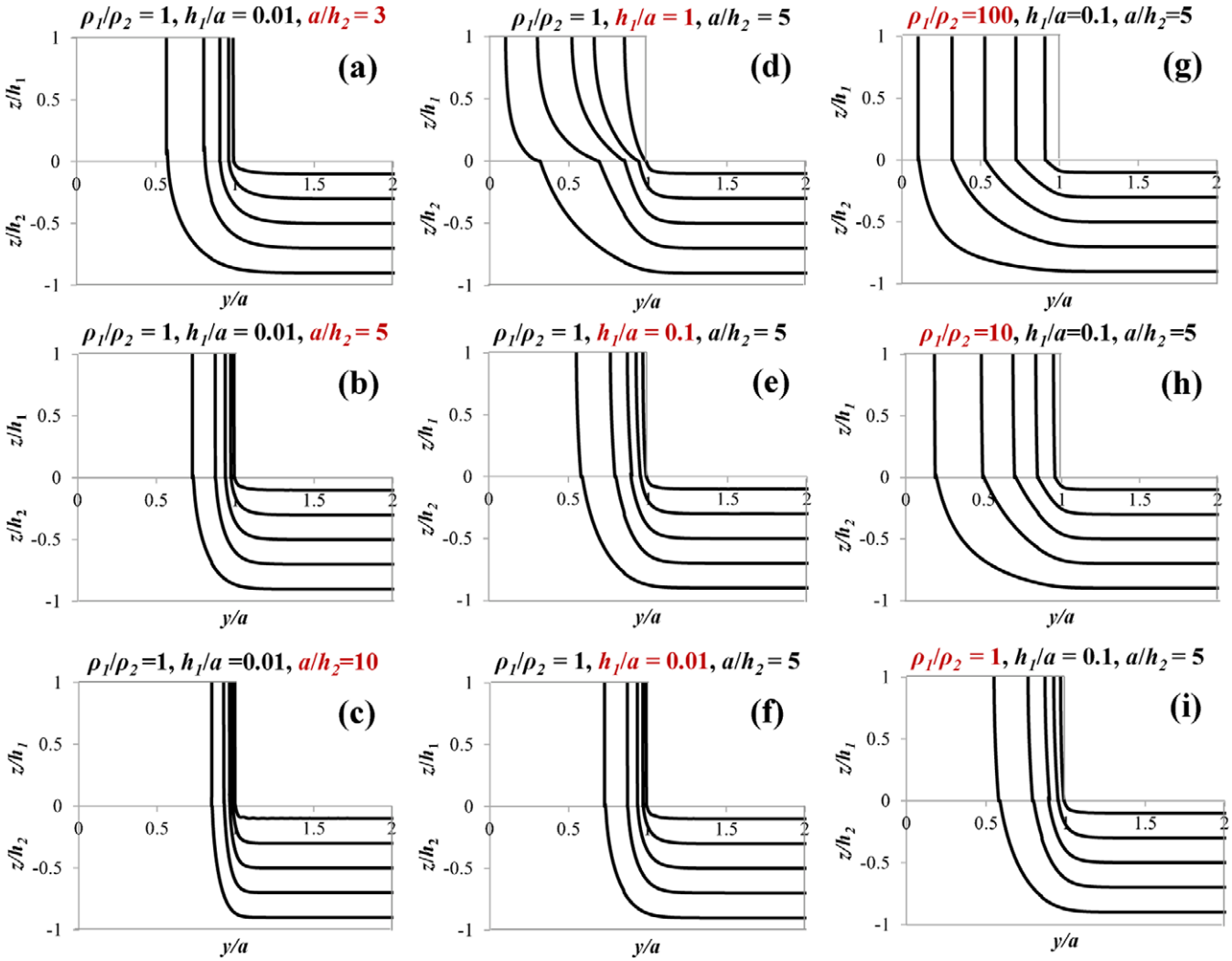

Figure 6. Field lines calculated from equation (A1) for the right half of the even solution of the Cartesian thin film contact (figure 2), for (*a*)–(*c*) $\rho_1/\rho_2 = 1$ and $h_1/a = 0.01$ with various a/h_2; (*d*)–(*f*) $\rho_1/\rho_2 = 1$ and $a/h_2 = 5$ with various h_1/a; and (*g*)–(*i*) and $h_1/a = 0.1$ and $a/h_2 = 5$ with various ρ_1/ρ_2.

The vast amount of data collected from the exact calculations allows us to synthesize a simple scaling law for $\bar{R}_c(O)$ as $h_1/a \to \infty$ in equation (B9), (for $b \gg a$ or $b \gg h_2$). This scaling law, equation (B9), is in excellent agreement with the exact calculation shown in figure 7 for the range $0 < \rho_1/\rho_2 < \infty$, $a/h_2 < 50$. Note that equation (4) also gives the limit of $h_1/a \to 0$. See comment (3) in the lead paragraph of section 2.

Figure 8 shows the exact theory of $\bar{R}_c(O)$ (see equation (B8)) as a function of a/h_2, for various ρ_1/ρ_2, addressing the effect of h_1/a in each sub-figure. For a given resistivity ratio ρ_1/ρ_2, $\bar{R}_c(O)$ increases as h_1/a increases at fixed a/h_2. The range of variation $\bar{R}_c(O)$ increases as a/h_2 increases. For each sub-figure of a given ρ_1/ρ_2 in figure 8, the bounds of the curves are governed by equations (4) and (B9), as explained in the preceding paragraph. (Equation (B9) is not shown in figure 8 because it coincides with the top solid line in each sub-figure.) If ρ_1/ρ_2 is small, as in figure 8(*a*) for $\rho_1/\rho_2 = 0.01$, h_1/a has little effect on $\bar{R}_c(O)$. As ρ_1/ρ_2 increases, the effect of h_1/a on $\bar{R}_c(O)$ is more pronounced. As ρ_1/ρ_2 increases, the curves for $\bar{R}_c(O)$ are shifting towards the upper bound, equation (3). The analytic calculations are confirmed with MAXWELL 2D simulation [17], shown by the symbols in figure 8.

From the exact expression of the potential everywhere, equation (B1), the current distribution may be readily evaluated. This is shown in figures 9 and 10. The current leaving terminal F, I_F, is split into three parts (GJ, JO, OK) of the grounded boundary GJK (figure 3). The three current fractions, I_{GJ}/I_F, I_{JO}/I_F and I_{OK}/I_F, may be calculated from equations (B6) and (B7) of appendix B. Examples of these current fractions as a function of a/h_2 are shown in figures 9(*a*)–(*c*) for $\rho_1/\rho_2 = 1$ with varying h_1/a, and in figures 9(*d*)–(*f*) for $h_1/a = 1$ with varying ρ_1/ρ_2. In general, I_{GJ}/I_F and I_{JO}/I_F increase as a function of a/h_2, whereas I_{OK}/I_F decrease as a function of a/h_2. For a fixed ρ_1/ρ_2, as h_1/a increases, I_{GJ}/I_F decreases, but I_{JO}/I_F and I_{OK}/I_F increase (figures 9(*a*)–(*c*)). For a fixed h_1/a, as ρ_1/ρ_2 increases, I_{GJ}/I_F and I_{JO}/I_F decrease, but I_{OK}/I_F increases (figures 9(*d*)–(*f*)). Note that the sum of current fraction $I_{GJ}/I_F + I_{JO}/I_F + I_{OK}/I_F = 1$, as expected.

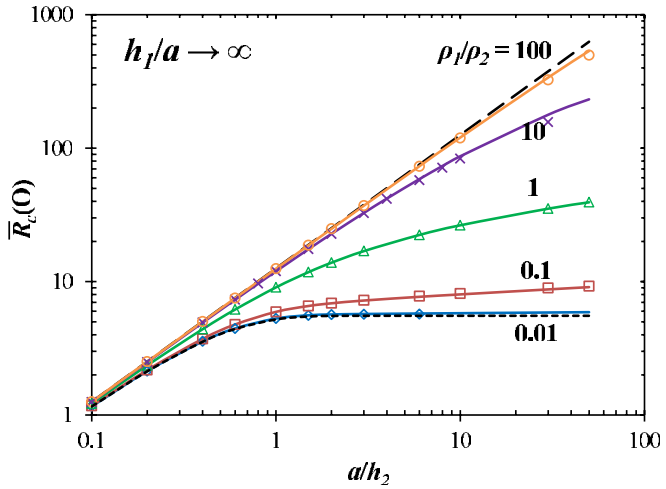

Figure 7. $\bar{R}_c(O)$ in the limit of $h_1/a \to \infty$, for the odd solution of Cartesian thin film contact (figure 3). The solid lines represent the synthesized scaling law (equation (B9)), symbols represent the exact calculations (equation (B8)) and the upper and lower dashed lines represent the limiting cases, respectively, of $\rho_1/\rho_2 \to \infty$ (equation (3)), and of $\rho_1/\rho_2 \to 0$ (equation (4)).

The field line equation, $y = y(z)$, may be numerically integrated from the first-order ordinary differential equation $\mathrm{d}y/\mathrm{d}z = E_y/E_z = (\partial\Phi/\partial y)/(\partial\Phi/\partial z)$ where Φ is given by equation (B1). The field lines in the right half of the thin film structure (figure 3) are shown for the special cases of $\rho_1/\rho_2 = 1$ and $h_1/a = 0.01$ with various a/h_2 in figures 10(*a*)–(*c*); $\rho_1/\rho_2 = 1$ and $a/h_2 = 5$ with various h_1/a in figures 10(*d*)–(*f*); and $h_1/a = 0.1$ and $a/h_2 = 5$ with various ρ_1/ρ_2 in figures 10(*g*)–(*i*). It is clear that as a/h_2 increases, the field lines (also the current flow lines) are more crowded towards the constriction corner B, as shown in figures 10(*a*)–(*c*), indicating more enhanced local heating. For small h_1/a (figure 10(*f*)), GJ is about to touch the interface OB, and the fringe fields at corner B provide severe current crowding. As h_1/a increases, the field lines across the interface OB become more uniformly distributed, as shown in figures 10(*e*) and (*d*). As h_1/a further increases (not shown), the region from BO to GJ becomes more resistive, and the current flows mostly across the vertical axis JO and OK. This explains the trend shown in figures 10(*d*)–(*f*). As ρ_1/ρ_2 increases, the field lines across the interface BO in region BOJG become more uniformly distributed, as shown in figures 10(*g*)–(*i*). As ρ_1/ρ_2 further increases, as shown in figure 10(*g*), region BOJG becomes more resistive, resulting in current flows across the vertical interface OK. This behaviour is again consistent with the current fraction results shown in figure 9(*f*).

3. Circular thin film contact

For the circular thin film contact that is also represented in figure 2, the top terminal GH is grounded and the rim of the circular disc (E and F) is biased at V_0. Comments (1)–(3) at the beginning of section 2 also apply to the circular thin film contact. All current flowing from the circular rim EF ends up at the gate GH. The total current that reaches the gate is

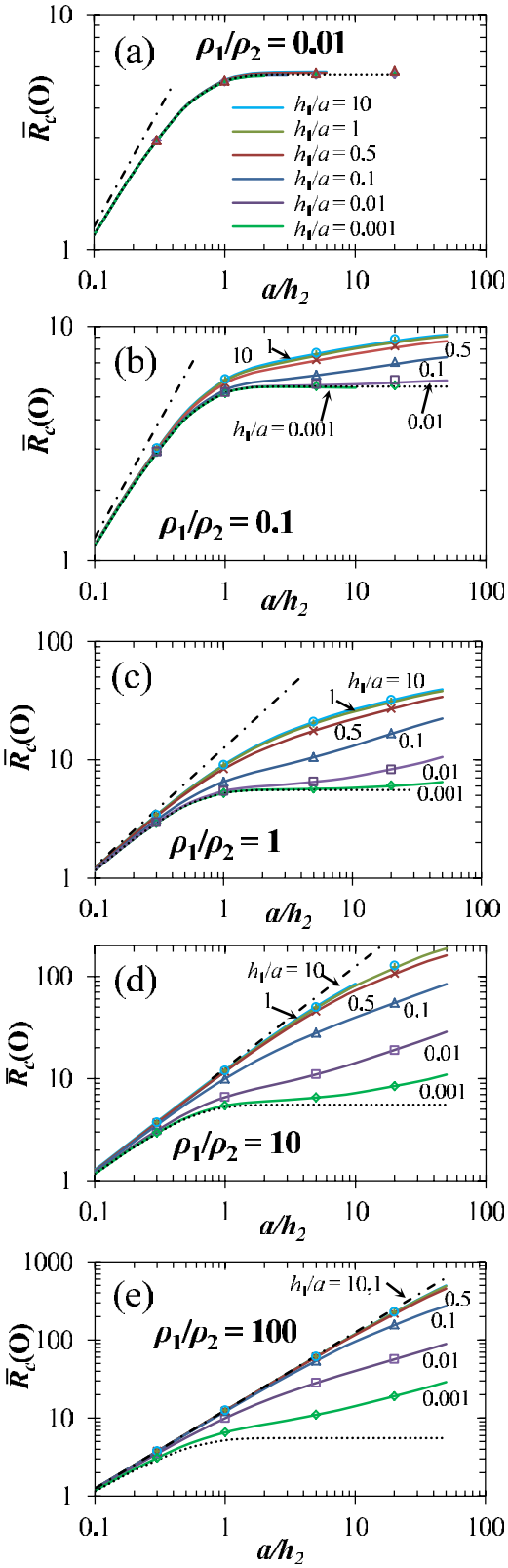

Figure 8. $\bar{R}_c(O)$ as a function of a/h_2, for $\rho_1/\rho_2 = 0.01$ (*a*), 0.1 (*b*), 1 (*c*), 10 (*d*), and 100 (*e*), with the effect of h_1/a displayed in each sub-figure. The solid lines represent the exact calculations (equation (B8)), symbols represent MAXWELL 2D simulation, the dashed–dotted lines represent equation (3), and dotted lines represent equation (4).

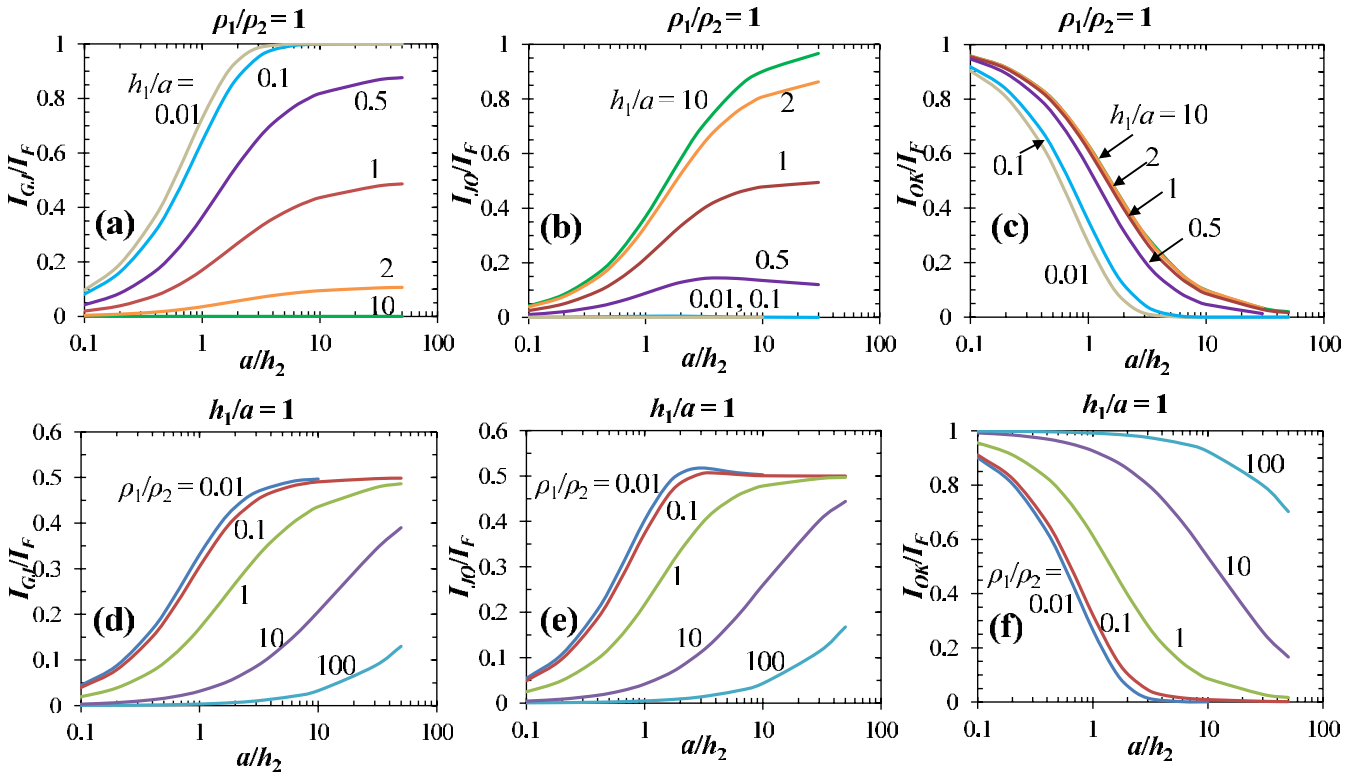

Figure 9. Current fractions of the odd solution of figure 3, as a function of a/h_2, (a)–(c) for $\rho_1/\rho_2 = 1$ with varying h_1/a, (d)–(f) for $h_1/a = 1$ with varying ρ_1/ρ_2.

$I_{\text{gate}} = V_0/R$, where R is the resistance from the circular rim E(F) to the gate GH and is found to be

$$R = \frac{\rho_2}{2\pi h_2}\ln\left(\frac{b}{a}\right) + \frac{\rho_2}{4a}\bar{R}_c\left(\frac{a}{b}, \frac{h_1}{a}, \frac{a}{h_2}, \frac{\rho_1}{\rho_2}\right) + \frac{\rho_1 h_1}{\pi a^2}. \quad (5)$$

In equation (5), the first term represents the bulk resistance of the thin film in region II, exterior to the constriction region ABCD [13, 15, 19]. The third term represents the bulk resistance of the top cylinder, BCHG. The second term represents the remaining constriction resistance, R_c, for region ABCD, and is expressed as $R_c = (\rho_2/4a)\bar{R}_c$ for the circular case. The normalized $\bar{R}_c$ depends on the aspect ratios a/b, h_1/a, a/h_2, and on the resistivity ratio ρ_1/ρ_2, as explicitly shown in equation (5). The *exact* expression for $\bar{R}_c$ is derived in appendix C (see equation (C6)). Again, we assume $b \gg a$ or $b \gg h_2$, in which case $\bar{R}_c$ is independent of b [13], as explained for the Cartesian case.

The cylindrical $\bar{R}_c$ (see equation (C6)) for the limiting case of $h_1/a \to \infty$ has been studied in detail in [13], which was fitted to a simple scaling law (equation (C7) of appendix C), plotted as a function of a/h_2 at various values of ρ_1/ρ_2 in figure 11. This scaling law is more accurate than the one given in [13]. In the opposite limit $h_1/a \to 0$, $\bar{R}_c$ is given by equation (C10). These two equations (C7) and (C10), define the bounds on each sub-figure in figure 12. Figure 12 shows the exact theory of $\bar{R}_c$ (see equation (C6)) as a function of a/h_2, for various ρ_1/ρ_2, and h_1/a, which exhibits similar properties to the even solution of the Cartesian case (figure 5). The calculations are confirmed with MAXWELL 2D simulation results [17], shown by the symbols in figure 12. We found that the electric field patterns for this cylindrical case are very similar to figure 6, a property anticipated from a previous paper [15].

4. Concluding remarks

This paper presents accurate analytical models on 3-terminal thin film contact with dissimilar materials. The models assume arbitrary geometric dimensions and arbitrary resistivities in the individual contact members, as well as arbitrary terminal voltages. The general Cartesian 3-terminal thin film contact is decomposed into the even and odd cases, both of which are solved exactly by the series expansion method. The even solution gives exclusively the current flowing from the source to the gate. The odd solution gives exclusively the current flowing from the source to the drain. Both the current flow patterns and the contact resistances are calculated. The contact resistances are validated against the MAXWELL code. Current partition in different regions is also calculated. Our analysis implies that the highest current density occurs at the contact corner (point B in figure 1) on the 'source' side, indicating the highest power density dissipation and therefore the hottest temperature spot there. The bounds on the variation of the contact resistance are obtained for both the even and odd solutions. No general scaling laws have been constructed for figures 5, 8 and 12, despite our considerable efforts, due to the huge parameter space. The bounds on these figures were established, however.

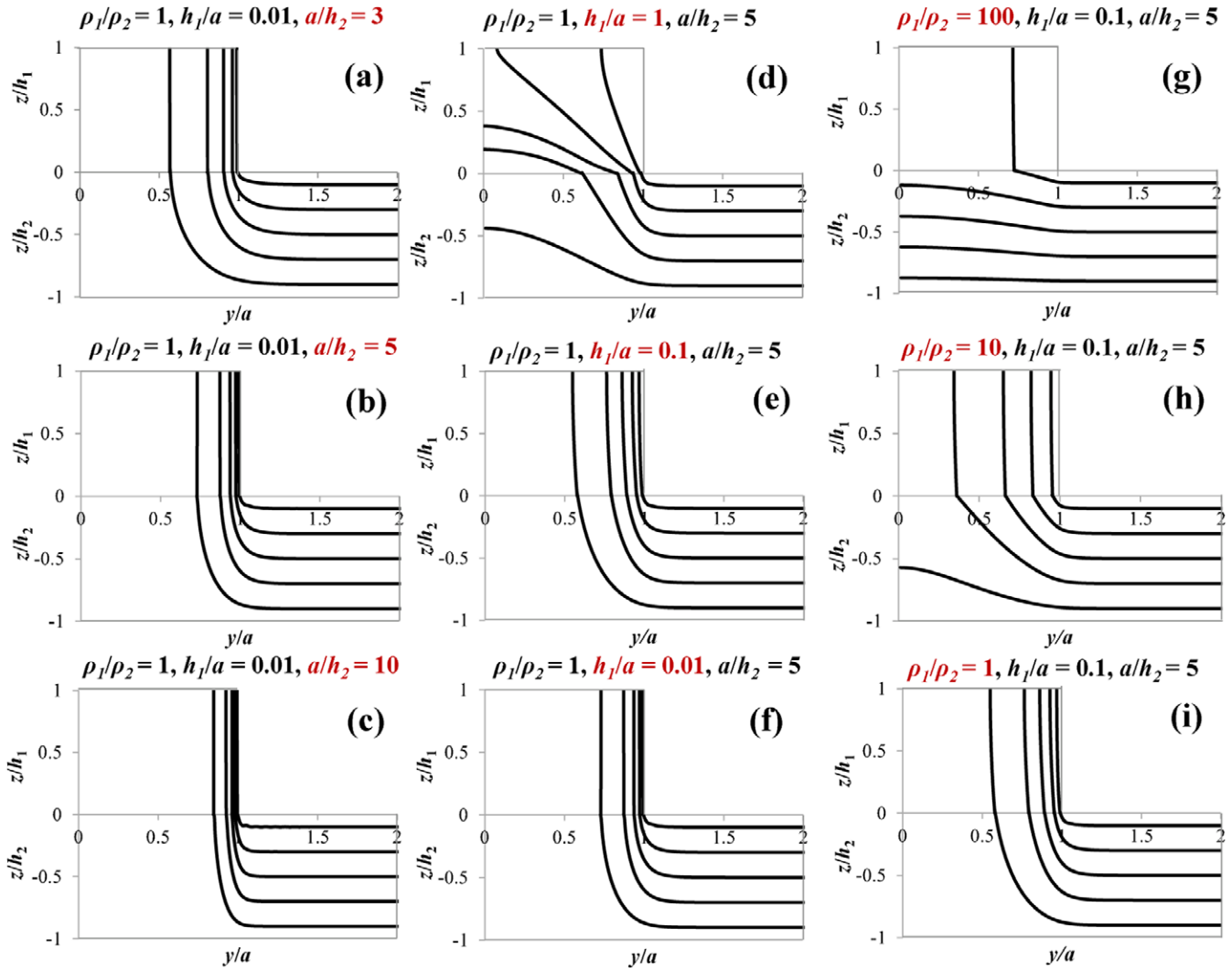

Figure 10. Field lines calculated from equation (B1) for the right half of the odd solution of the Cartesian thin film contact (figure 3), for (*a*)–(*c*) $\rho_1/\rho_2 = 1$ and $h_1/a = 0.01$ with various a/h_2; (*d*)–(*f*) $\rho_1/\rho_2 = 1$ and $a/h_2 = 5$ with various h_1/a; and (*g*)–(*i*) and $h_1/a = 0.1$ and $a/h_2 = 5$ with various ρ_1/ρ_2.

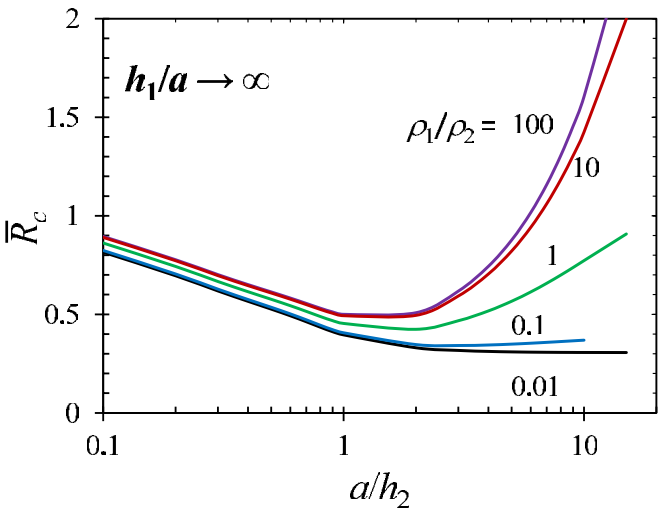

Figure 11. $\bar{R}_c$ in the limit of $h_1/a \to \infty$, for circular thin film contact (figure 2). The curves represent the synthesized scaling law (equation (C7)).

In figure 1, the current flow at terminal F is assumed to be uniform, an assumption easily satisfied from the flow patterns displayed in figures 6 and 10. We now extend the y-coordinate of terminal F to a new position F', say, at $y = b'$, while the coordinates of, and the voltages at, terminals E and GH remain unchanged. Identical current flow patterns would be obtained if we simply set the voltage at F' equal to $V_R + I_F\rho_2(b' - b)/(Wh_2)$ where I_F is the total current flowing through terminal F (or F'). Thus, for the Cartesian thin film model shown in figure 1, we have generalized the analysis presented in this paper, further, to the non-symmetric geometry where region I need not be placed at the centre of region II. Our model then provides a substantial generalization of the transmission line model and the Kennedy–Murley model that were extensively used in thin film analysis.

Acknowledgments

This work was supported by an AFOSR grant on the Basic Physics of Distributed Plasma Discharge, AFOSR grant

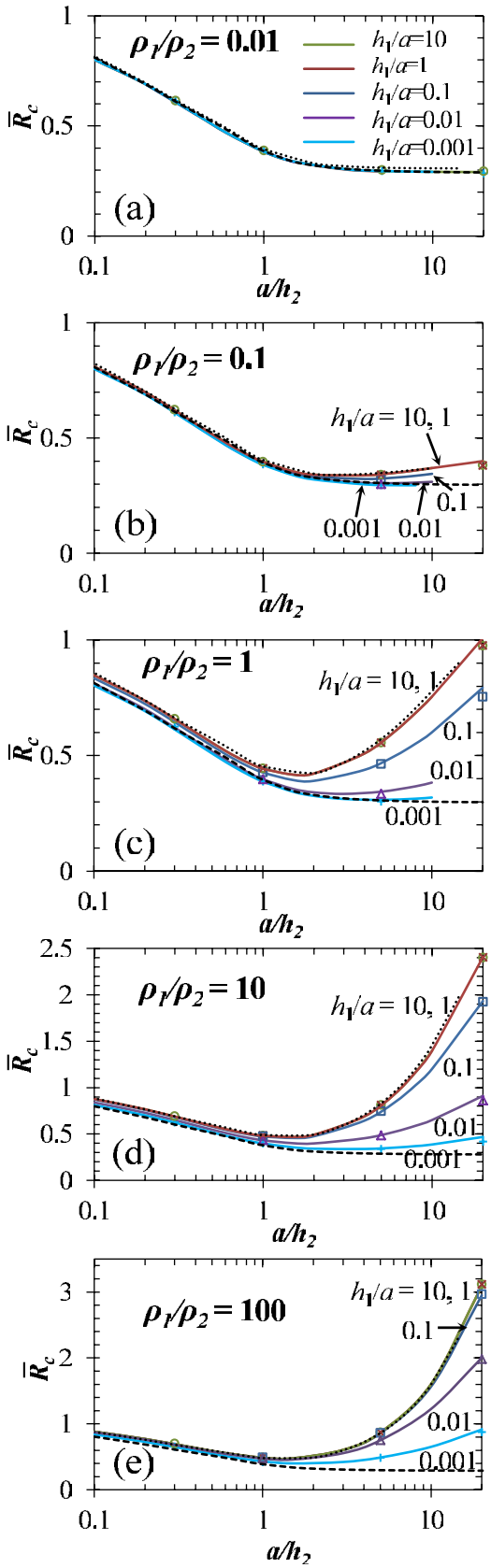

Figure 12. $\bar{R}_c$ for circular thin film contact (figure 2) as a function of a/h_2, for $\rho_1/\rho_2 = 0.01$ (*a*), 0.1 (*b*), 1 (*c*), 10 (*d*) and 100 (*e*), with the effect of h_1/a displayed in each sub-figure. The solid lines represent the exact calculations (equation (C6)), symbols represent MAXWELL 2D simulation, the dotted lines represent equation (C7) and the dashed lines represent equation (C10).

FA9550-09-1-0662, L-3 Communications Electron Device Division, and Northrop-Grumman Corporation.

Appendix A. General solution to the Cartesian even case (figure 2)

The formulation follows that of [12, 13]. Referring to figure 2, a voltage of $+V_0$ is applied at both the right and left terminals. The solutions to Laplace's equation are [13],

$$\Phi_+(y,z) = A_0(z-h_1) + \sum_{n=1}^{\infty} A_n \cos\left(\frac{n\pi y}{a}\right) \times \sinh\left(n\pi\frac{z-h_1}{a}\right), \qquad 0 < z < h_1,\ |y| \in (0,a),$$

$$\Phi_-(y,z) = V_0 + \sum_{n=1}^{\infty} B_n \cos\left(\left(n-\frac{1}{2}\right)\pi\frac{y}{b}\right) \times \frac{\cosh\left[\left(n-\frac{1}{2}\right)\pi\frac{z+h_2}{b}\right]}{\sinh\left(\left(n-\frac{1}{2}\right)\pi\frac{h_2}{b}\right)}, \qquad -h_2 < z < 0,\ |y| \in (0,b), \tag{A1}$$

where Φ_+ and Φ_- are the electrical potential in regions BCHG and BCEF, respectively, and A_n and B_n are the coefficients that need to be solved.

At the interface $z = 0$, from the continuity of electrical potential and current density, we have the following boundary conditions:

$$\Phi_+ = \Phi_-, \qquad z = 0, \quad |y| \in (0,a), \tag{A2a}$$

$$\frac{1}{\rho_1}\frac{\partial\Phi_+}{\partial z} = \frac{1}{\rho_2}\frac{\partial\Phi_-}{\partial z}, \qquad z = 0, \quad |y| \in (0,a), \tag{A2b}$$

$$\frac{\partial\Phi_-}{\partial z} = 0, \qquad z = 0, \quad |y| \in (a,b). \tag{A2c}$$

From equations (A2a)–(A2c), we eliminate coefficient A_n in favour of B_n to obtain

$$-A_n \sinh\left(n\pi\frac{h_1}{a}\right) = \sum_{m=1}^{\infty} g_{mn} B_m \coth\left((m-1/2)\,\pi\frac{h_2}{b}\right), \tag{A3a}$$

$$\frac{\rho_1}{\rho_2}(n-1/2)B_n + \sum_{m=1}^{\infty}\gamma_{nm}B_m \coth\left((m-1/2)\pi\frac{h_2}{b}\right) = \frac{2}{\pi}\frac{\sin((n-1/2)\pi a/b)}{(n-1/2)\pi a/b}, \qquad n = 1,2,3\ldots, \tag{A3b}$$

where

$$\gamma_{nm} = \gamma_{mn} = \sum_{l=1}^{\infty} l g_{nl} g_{ml} \coth\left(\frac{l\pi h_1}{a}\right),$$

$$g_{mn} = \frac{2}{a}\int_0^a \mathrm{d}y \cos\left(\frac{(m-1/2)\pi y}{b}\right)\cos\left(\frac{n\pi y}{a}\right). \tag{A4}$$

In deriving equation (A3b), we have assumed that $aA_0 = +1$. The infinite matrix in equation (A3b) can be solved directly for B_n with convergence guaranteed, from which A_n follows

in equation (A3a). See the appendices of [12, 13] for the proof of convergence.

The total current flowing to the gate GH is (figure 2)

$$I = 2W \int_0^a \frac{1}{\rho_1} \frac{\partial \Phi_+}{\partial z}\bigg|_{z=0} \mathrm{d}y = \frac{2W}{\rho_1}, \tag{A5}$$

where we have used equation (A1) and $aA_0 = +1$, and W is the channel width in the third, ignorable dimension that is perpendicular to the paper. The terminal voltage V_0 may be expressed in terms of B_n as

$$V_0 = -\frac{h_1}{a} - \sum_{n=1}^{\infty} B_n \coth\left((n-1/2)\pi\frac{h_2}{b}\right) \times \frac{\sin\left((n-1/2)\pi a/b\right)}{(n-1/2)\pi a/b}. \tag{A6}$$

The contact resistance for this even case, $R_c(\mathrm{E})$, is defined as the difference between the resistance from EF to GH, $R = V_0/I$, and the bulk resistance exterior to ABCD, $R_u = \rho_1 h_1/2aW + \rho_2(b-a)/2h_2W$,

$$\begin{aligned} R_c(\mathrm{E}) &\equiv \frac{\rho_2}{4\pi W}\bar{R}_c(\mathrm{E}) = \frac{V_0}{I} - R_u, \\ \bar{R}_c(E) &= \bar{R}_c(E)\left(\frac{a}{b}, \frac{h_1}{a}, \frac{a}{h_2}, \frac{\rho_1}{\rho_2}\right) \\ &= 2\pi\frac{\rho_1}{\rho_2}\sum_{n=1}^{\infty} B_n \coth\left(\left(n-\frac{1}{2}\right)\pi\frac{h_2}{b}\right) \\ &\quad \times \frac{\sin\left(\left(n-\frac{1}{2}\right)\pi\frac{a}{b}\right)}{\left(n-\frac{1}{2}\right)\pi\frac{a}{b}} - 2\pi\frac{b-a}{h_2}. \end{aligned} \tag{A7}$$

Equation (A7) is the *exact* expression for the contact resistance of Cartesian thin film of the even case (figure 2) for arbitrary values of a, b ($b > a$), h_1, h_2 and ρ_1/ρ_2. In equation (A7), B_n is solved from equation (A3b). Equation (A7) appears in equation (1) of the main text.

In the limit $h_1/a \to \infty$, $\bar{R}_c(E)$ according to the exact theory (A7) is plotted in figure 4 of the main text. The exact theory in figure 4 may be fitted by equation (A8), which is more accurate and elegant than the fitting formula given in [13],

$$\bar{R}_c(\mathrm{E})\left(\frac{a}{h_2}, \frac{\rho_1}{\rho_2}\right) \cong \bar{R}_c(\mathrm{E})\big|_{\frac{\rho_1}{\rho_2}\to 0} + \frac{\Delta(a/h_2)}{2} \times \frac{2\rho_1}{\rho_1 + \beta(a/h_2)\rho_2}, \qquad h_1/a \to \infty, \tag{A8}$$

where

$$\Delta(a/h_2) = \bar{R}_c(\mathrm{E})\big|_{\rho_1/\rho_2\to\infty} - \bar{R}_c(\mathrm{E})\big|_{\rho_1/\rho_2\to 0}, \tag{A9}$$

$$\beta(a/h_2) = \frac{\bar{R}_c(\mathrm{E})\big|_{\rho_1/\rho_2\to\infty} - \bar{R}_c(\mathrm{E})\big|_{\rho_1/\rho_2=1}}{\bar{R}_c(\mathrm{E})\big|_{\rho_1/\rho_2=1} - \bar{R}_c(\mathrm{E})\big|_{\rho_1/\rho_2\to 0}}, \tag{A10}$$

$$\bar{R}_c(E)\big|_{\frac{\rho_1}{\rho_2}\to 0} = 2\pi\frac{a}{h_2} - 4\ln\left[\sinh\left(\frac{\pi}{2}\frac{a}{h_2}\right)\right], \tag{A11}$$

$$\bar{R}_c(\mathrm{E})\big|_{\frac{\rho_1}{\rho_2}=1} = 4\ln\left[\frac{1}{4}\left(\frac{a}{h_2} + \frac{h_2}{a}\right)\right] + 4\left(\frac{h_2}{a}\right)\tan^{-1}\left(\frac{a}{h_2}\right) + 4\left(\frac{a}{h_2}\right)\tan^{-1}\left(\frac{h_2}{a}\right), \tag{A12}$$

$$\bar{R}_c(\mathrm{E})\big|_{\frac{\rho_1}{\rho_2}\to\infty} \cong \begin{cases} \bar{R}_c(\mathrm{E})\big|_{\frac{\rho_1}{\rho_2}\to 0} + 0.5355(a/h_2)^2 \\ \quad + 0.006594(a/h_2) + 0.4546, & a/h_2 \leqslant 1; \\ \frac{2}{3}\pi(a/h_2) + 2.094(h_2/a) \\ \quad - 0.2429(h_2/a)^2, & a/h_2 > 1. \end{cases} \tag{A13}$$

The fitting formula (A8) is expressed in terms of $\bar{R}_c(E)$ in the three important limits: $\rho_1/\rho_2 = 0$, 1, and infinity. Equations (A11) and (A12) may be obtained from Hall [18], whereas equation (A13) is an excellent approximation to the exact expression, given by equation (A10) of [13],

$$\bar{R}_c(\mathrm{E})\big|_{\frac{\rho_1}{\rho_2}\to\infty} = 4\sum_{n=1}^{\infty}\frac{\coth\left[\left(n-\frac{1}{2}\right)\pi\frac{h_2}{b}\right]}{n-\frac{1}{2}}\frac{\sin^2\left[\left(n-\frac{1}{2}\right)\pi\frac{a}{b}\right]}{\left[\left(n-\frac{1}{2}\right)\pi\frac{a}{b}\right]^2} - 2\pi\frac{b-a}{h_2}. \tag{A14}$$

As $h_2 \to 0$, equation (A14) yields the asymptotic limit $(2\pi/3)(a/h_2)$, which is displayed in equation (A13). See appendix C of [16] for a mathematical proof of this asymptotic limit. From comment (3) in the lead paragraph of section 2, equation (A11) is also the expression in the limit $h_1/a \to 0$,

$$\bar{R}_c(\mathrm{E}) = 2\pi\frac{a}{h_2} - 4\ln\left[\sinh\left(\frac{\pi}{2}\frac{a}{h_2}\right)\right], \qquad h_1/a \to 0. \tag{A15}$$

Appendix B. General solution to the Cartesian odd case (figure 3)

In figure 3, we set the voltage $V_0' = 1$ for this appendix where we calculate the contact resistance and the *ratios* of various current components. The solutions of Laplace's equation are

$$\begin{aligned} \Phi_+(y,z) &= \sum_{n=1}^{\infty} A_n \sin\left(\left(n-\frac{1}{2}\right)\pi\frac{y}{a}\right) \\ &\quad \times \sinh\left(\left(n-\frac{1}{2}\right)\pi\frac{z-h_1}{a}\right), \\ &\quad 0 < z < h_1, \ |y| \in (0,a), \\ \Phi_-(y,z) &= \frac{y}{b} + \sum_{n=1}^{\infty} B_n \sin\left(\frac{n\pi y}{b}\right)\frac{\cosh[(z+h_2)n\pi/b]}{\sinh(n\pi h_2/b)}, \\ &\quad -h_2 < z < 0, \ |y| \in (0,b), \end{aligned} \tag{B1}$$

where Φ_+ and Φ_- are the electrical potential in regions BCHG and BCEF, respectively, and A_n and B_n are the coefficients that need to be solved.

At the interface $z = 0$, from the continuity of electrical potential and current density, we have the following boundary conditions:

$$\Phi_+ = \Phi_-, \qquad z = 0, \ |y| \in (0,a), \tag{B2a}$$

$$\frac{1}{\rho_1}\frac{\partial\Phi_+}{\partial z} = \frac{1}{\rho_2}\frac{\partial\Phi_-}{\partial z}, \qquad z = 0, \ |y| \in (0,a), \tag{B2b}$$

$$\frac{\partial\Phi_-}{\partial z} = 0, \qquad z = 0, \ |y| \in (a,b). \tag{B2c}$$

From equations (B1) and (B2a), the coefficient A_n is expressed in terms of B_n,

$$-A_n \sinh\left(\frac{(n-1/2)\pi h_1}{a}\right) = 2\frac{a}{b}\frac{\sin((n-1/2)\pi)}{((n-1/2)\pi)^2} + \sum_{m=1}^{\infty} B_m \coth\left(\frac{m\pi h_2}{b}\right) g_{mn}, \qquad n \geqslant 1$$

$$g_{mn} = \frac{1}{a}\int_{-a}^{a} \mathrm{d}y \sin\left(\frac{m\pi y}{b}\right)\sin\left(\frac{(n-1/2)\pi y}{a}\right). \tag{B3}$$

Combining equations (B2b), (B2c) and (B3), we obtain

$$\frac{\rho_1}{\rho_2} n B_n + \sum_{m=1}^{\infty} \gamma_{nm} B_m \coth\left(\frac{m\pi h_2}{b}\right) = -\frac{2}{\pi}\frac{a}{b} D_n, \quad n = 1, 2, 3\ldots, \tag{B4}$$

where

$$\gamma_{nm} = \gamma_{mn} = \sum_{l=1}^{\infty} (l-1/2)\, g_{nl} g_{ml} \coth\left(\frac{(l-1/2)\pi h_1}{a}\right),$$

$$D_n = \sum_{l=1}^{\infty} g_{nl} \coth\left(\frac{(l-1/2)\pi h_1}{a}\right)\frac{\sin((l-1/2)\pi)}{(l-1/2)\pi}, \tag{B5}$$

in which g_{nl} and g_{ml} are in the form of the last part in equation (B3). The infinite matrix (B4) can be solved directly for B_n with convergence guaranteed. See the appendices of [12, 13] for the proof of convergence.

The total current from the right terminal, F, is

$$I_{\mathrm{F}} = W\int_{-h_2}^{0} \frac{1}{\rho_2}\frac{\partial \Phi_-}{\partial y}\bigg|_{y=b} \mathrm{d}z = \frac{W}{\rho_2}\left(\frac{h_2}{b} + \sum_{n=1}^{\infty} B_n \cos(n\pi)\right), \tag{B6}$$

where we have used equation (B1). This current is split into three parts (GJ, JO, OK) when it reaches the grounded boundary GJK in figure 3,

$$I_{\mathrm{GJ}} = W\int_{0}^{a} \frac{1}{\rho_1}\frac{\partial \Phi_+}{\partial z}\bigg|_{z=h_1} \mathrm{d}y = \frac{W}{\rho_1}\sum_{n=1}^{\infty} A_n,$$

$$I_{\mathrm{JO}} = W\int_{0}^{h_1} \frac{1}{\rho_1}\frac{\partial \Phi_+}{\partial y}\bigg|_{y=0} \mathrm{d}z = \frac{W}{\rho_1}\sum_{n=1}^{\infty} A_n\left[1 - \cosh\left(\frac{(n-1/2)\pi h_1}{a}\right)\right],$$

$$I_{\mathrm{OK}} = W\int_{-h_2}^{0} \frac{1}{\rho_2}\frac{\partial \Phi_-}{\partial y}\bigg|_{y=0} \mathrm{d}z = \frac{W}{\rho_2}\left(\frac{h_2}{b} + \sum_{n=1}^{\infty} B_n\right), \tag{B7}$$

where B_n and A_n are solved from equations (B4) and (B3), respectively.

The contact resistance for this odd case, $R_{\mathrm{c}}(\mathrm{O})$, is defined as the difference between the resistance from terminal F to the grounded boundary GJK, $R = 1/I_{\mathrm{F}}$, and the bulk resistance between AB and terminal F, $R_{\mathrm{u}} = \rho_2(b-a)/h_2 W$,

$$R_{\mathrm{c}}(\mathrm{O}) \equiv \frac{\rho_2}{4\pi W}\bar{R}_{\mathrm{c}}(\mathrm{O}) = \frac{1}{I_{\mathrm{F}}} - \frac{\rho_2(b-a)}{h_2 \times W},$$

$$\bar{R}_{\mathrm{c}}(\mathrm{O}) = \bar{R}_{\mathrm{c}}(\mathrm{O})\left(\frac{a}{b}, \frac{h_1}{a}, \frac{a}{h_2}, \frac{\rho_1}{\rho_2}\right) = \frac{4\pi}{\frac{h_2}{b} + \sum_{n=1}^{\infty} B_n \cos(n\pi)} - 4\pi\frac{b-a}{h_2}. \tag{B8}$$

Equation (B8) is the *exact* expression for the contact resistance of Cartesian thin film of the odd case (figure 3) for arbitrary values of a, b ($b > a$), h_1, h_2 and ρ_1/ρ_2. In equation (B8), B_n is solved from equation (B4). Equation (B8) appears in equation (2) of the main text.

In the limit $h_1/a \to \infty$, $\bar{R}_{\mathrm{c}}(\mathrm{O})$ according to the exact theory (B8) is plotted in figure 7 of the main text. The curves in figure 7 may be fitted by this formula,

$$\bar{R}_{\mathrm{c}}(\mathrm{O}) = \bar{R}_{\mathrm{c}}(\mathrm{O})\big|_{\rho_1/\rho_2\to 0} + \frac{\Delta(a/h_2)}{2} \times \frac{2\rho_1}{\rho_1 + \beta(a/h_2)\rho_2}, \tag{B9}$$

$$\Delta(a/h_2) = \bar{R}_{\mathrm{c}}(\mathrm{O})\big|_{\rho_1/\rho_2\to\infty} - \bar{R}_{\mathrm{c}}(\mathrm{O})\big|_{\rho_1/\rho_2\to 0},$$

$$\beta(a/h_2) = \frac{\bar{R}_{\mathrm{c}}(\mathrm{O})\big|_{\rho_1/\rho_2\to\infty} - \bar{R}_{\mathrm{c}}(\mathrm{O})\big|_{\rho_1/\rho_2=1}}{\bar{R}_{\mathrm{c}}(\mathrm{O})\big|_{\rho_1/\rho_2=1} - \bar{R}_{\mathrm{c}}(\mathrm{O})\big|_{\rho_1/\rho_2\to 0}}, \tag{B10}$$

where $\bar{R}_{\mathrm{c}}(\mathrm{O})|_{\rho_1/\rho_2\to\infty}$ and $\bar{R}_{\mathrm{c}}(\mathrm{O})|_{\rho_1/\rho_2\to 0}$ are given in equations (3) and (4) in the main text, respectively, and $\bar{R}_{\mathrm{c}}(\mathrm{O})|_{\rho_1/\rho_2=1}$ is given by

$$\bar{R}_{\mathrm{c}}(\mathrm{O})|_{\rho_1/\rho_2=1} = 4\pi\frac{a}{h_2} + 4\ln\left(\frac{a^2}{h_2^2}+1\right) - 8\frac{a}{h_2}\tan^{-1}\left(\frac{a}{h_2}\right), \tag{B11}$$

which is derived by Hall using conformal mapping (see figure 33 and equation (48) of Hall's 1967 paper [18]). This scaling law, equation (B9), is also shown in figure 7, which compares extremely well with the exact theory, for the range of $0 < \rho_1/\rho_2 < \infty$ and $a/h_2 \leqslant 50$.

Appendix C. General solution to the cylindrical case (figure 2)

The solutions of Laplace's equation in the cylindrical geometry are [13]

$$\Phi_+(r,z) = A_0(z-h_1) + \sum_{n=1}^{\infty} A_n J_0(\alpha_n r)\sinh[\alpha_n(z-h_1)], \quad 0 < z < h_1, r \in (0,a);$$

$$\Phi_-(r,z) = V_0 + \sum_{n=1}^{\infty} B_n \frac{\cosh((z+h_2)\lambda_n/b)}{\sinh(h_2\lambda_n/b)} J_0\left(\frac{\lambda_n r}{b}\right), \quad -h_2 < z < 0, r \in (0,b), \tag{C1}$$

where Φ_+ and Φ_- are the electrical potential in regions BCHG and BCEF, respectively, (figure 2), α_n and λ_n satisfy $J_1(\alpha_n a) = J_0(\lambda_n) = 0$, $J_0(x)$ and $J_1(x)$ is, respectively, the Bessel function of order zero and one, and A_n and B_n are the coefficients that need to be solved.

At the interface $z = 0$, from the continuity of electrical potential and current density, we have the following boundary conditions:

$$\Phi_+ = \Phi_-, \qquad z = 0, r \in (0,a), \tag{C2a}$$

$$\frac{1}{\rho_1}\frac{\partial \Phi_+}{\partial z} = \frac{1}{\rho_2}\frac{\partial \Phi_-}{\partial z}, \qquad z = 0,\ r \in (0,a), \tag{C2b}$$

$$\frac{\partial \Phi_-}{\partial z} = 0, \qquad z = 0,\ r \in (a,b). \tag{C2c}$$

From equations (C1) and (C2a), the coefficient A_n is expressed in terms of B_n,

$$-A_0 h_1 = \sum_{n=1}^{\infty} B_n \coth\left(\frac{\lambda_n h_2}{b}\right) \frac{2J_1(\lambda_n a/b)}{\lambda_n a/b} + V_0, \tag{C3a}$$

$$-\sinh(\alpha_n h_1) A_n = \sum_{m=1}^{\infty} B_m \coth\left(\frac{\lambda_m h_2}{b}\right) g_{mn},$$

$$g_{mn} = \frac{2}{a^2 J_0^2(\alpha_n a)} \int_0^a r\,\mathrm{d}r\, J_0(\alpha_n r)\, J_0\left(\frac{\lambda_m r}{b}\right), \qquad n \geqslant 1. \tag{C3b}$$

Combining equations (C2b), (C2c) and (C3b), we obtain

$$\frac{\rho_1}{\rho_2}\frac{b}{a}\lambda_n J_1^2(\lambda_n) B_n + \sum_{m=1}^{\infty} \gamma_{nm} B_m \coth\left(\frac{\lambda_m h_2}{b}\right) = \frac{2J_1(\lambda_n a/b)}{\lambda_n a/b}, \quad n = 1, 2, 3\ldots, \tag{C4}$$

where

$$\gamma_{nm} = \gamma_{mn} = \sum_{l=1}^{\infty} g_{nl} g_{ml} \alpha_l a J_0^2(\alpha_l a) \coth(\alpha_l h_1), \tag{C5}$$

in which g_{nl} and g_{ml} are in the form of the last part in equation (C3b). In deriving equation (C4), we have set $aA_0 = 1$ for simplicity.

The total resistance from the circular rim EF to GH is $R = (\Phi_F - \Phi_G)/I = V_0/I$, where $I = \int_0^a ((1/\rho_1)(\partial\Phi_+/\partial z)|_{z=0}) 2\pi r\,\mathrm{d}r = \pi a/\rho_1$ is the total current in the conducting channel. The contact resistance, R_c, is the difference between the total resistance R and bulk resistance in the region exterior to ABCD, $R_u = \rho_1 h_1/\pi a^2 + (\rho_2/2\pi h_2)\ln(b/a)$. We find

$$R_c = \frac{|V_0 - 0|}{I} - R_u = \frac{\rho_2}{4a}\bar{R}_c,$$

$$\bar{R}_c\left(\frac{a}{b}, \frac{h_1}{a}, \frac{a}{h_2}, \frac{\rho_1}{\rho_2}\right) = \frac{8}{\pi}\frac{\rho_1}{\rho_2}\sum_{n=1}^{\infty} B_n \coth(\lambda_n h_2/b)\frac{J_1(\lambda_n a/b)}{\lambda_n a/b} - \frac{2a}{\pi h_2}\ln\left(\frac{b}{a}\right), \tag{C6}$$

which is the *exact* expression for the circular thin film contact resistance with dissimilar materials for arbitrary values of a, b ($b > a$), h_1, h_2 and ρ_1/ρ_2. It appears in equation (5) of the main text. In equation (C6), B_n is solved from equation (C4).

In the limit $h_1/a \to \infty$, equations (C4)–(C6) become identical to equations (B6)–(B8) of [13]. The exact theory of $\bar{R}_c$ for the cylindrical case was fitted by equation (C7), which is more accurate and elegant than the fitting formula given in [13],

$$\bar{R}_c\left(\frac{a}{h_2}, \frac{\rho_1}{\rho_2}\right) \cong \bar{R}_c(a/h_2)\big|_{\frac{\rho_1}{\rho_2}\to 0} + \frac{\Delta(a/h_2)}{2} \times \frac{2\rho_1}{\rho_1 + \beta(a/h_2)\rho_2}, \qquad h_1/a \to \infty, \tag{C7}$$

where

$$\bar{R}_c(a/h_2)\big|_{\rho_1/\rho_2\to 0} = \begin{cases} 1 - 2.2968(a/h_2) + 4.9412(a/h_2)^2 \\ \quad - 6.1773(a/h_2)^3 \\ +3.811(a/h_2)^4 - 0.8836(a/h_2)^5, \\ \quad 0 \leqslant a/h_2 \leqslant 1; \\ 4\ln 2/\pi^2 + 0.055(h_2/a) \\ \quad +0.0541(h_2/a)^2, \\ \qquad 1 < a/h_2 < \infty, \end{cases} \tag{C8a}$$

$$\bar{R}_c(a/h_2)\big|_{\rho_1/\rho_2\to\infty} = \begin{cases} 1.0808 - 2.2895(a/h_2) \\ \quad +4.9596(a/h_2)^2 - 6.1773(a/h_2)^3 \\ +3.811(a/h_2)^4 - 0.8836(a/h_2)^5, \\ \quad 0 \leqslant a/h_2 \leqslant 1; \\ \frac{1}{2\pi}(a/h_2) + 0.4208(h_2/a) \\ \quad -0.0925(h_2/a)^2, \ 1 < a/h_2 < \infty, \end{cases} \tag{C8b}$$

$$\Delta(a/h_2) = \bar{R}_c(a/h_2)\big|_{\rho_1/\rho_2\to\infty} - \bar{R}_c(a/h_2)\big|_{\rho_1/\rho_2\to 0},$$
$$\beta(a/h_2) = 0.0016(a/h_2)^2 + 0.0949(a/h_2) + 0.6983, \quad 0.001 \leqslant a/h_2 < 10. \tag{C9}$$

As $h_2 \to 0$, the asymptotic limits displayed in equations (C8a) and (C8b) are demonstrated in [16]. From comment (3) in the lead paragraph of section 2, equation (C8a) is also the expression in the limit $h_1/a \to 0$,

$$\bar{R}_c(a/h_2)\big|_{h_1/a\to 0} = \begin{cases} 1 - 2.2968(a/h_2) + 4.9412(a/h_2)^2 \\ \quad - 6.1773(a/h_2)^3 \\ +3.811(a/h_2)^4 - 0.8836(a/h_2)^5, \\ \quad 0 \leqslant a/h_2 \leqslant 1; \\ 4\ln 2/\pi^2 + 0.055(h_2/a) \\ \quad +0.0541(h_2/a)^2, \\ \qquad 1 < a/h_2 < \infty. \end{cases} \tag{C10}$$

References

[1] Schroder D K 1998 *Semiconductor Material and Device Characterization* 2nd edn (New York: Wiley)

[2] Berger H H 1972 Models for contacts to planar devices *Solid State Electron.* **15** 145–58

[3] Grosse K L, Bae M, Lian F, Pop E and King W P 2011 Nanoscale Joule heating, Peltier cooling and current crowding at graphene–metal contacts *Nature Nanotechnol.* **6** 287–90

[4] Clem J R and Berggren K K 2011 Geometry-dependent critical currents in superconducting nanocircuits *Phys. Rev.* B **84** 174510

[5] Berger H H 1969 Contact resistance on diffused resistors *Dig. Tech. Pap. ISSCC* **XII** 160–1

[6] Murrmann H and Widmann D 1969 Current crowding on metal contacts to planer devices *Dig. Tech. Pap. ISSCC* **XII** 162–3

[7] Kennedy D P and Murley P C 1968 A two-dimensional mathematical analysis of the diffused semiconductor resistor *IBM J. Res. Dev.* **12** 242–50

[8] Holm R 1967 *Electric Contact* 4th edn (Berlin: Springer)
[9] Timsit R S 1999 Electrical contact: fundamental principles *Electrical Contacts: Principles and Applications* ed P G Slade (New York: Dekker)
[10] Timsit R S 1999 Electrical contact resistance: properties of stationary interfaces *IEEE Trans. Compon. Packag. Technol.* **22** 85
[11] Lau Y Y and Tang W 2009 A higher dimensional theory of electrical contact resistance *J. Appl. Phys.* **105** 124902
[12] Zhang P and Lau Y Y 2010 Scaling laws for electrical contact resistance with dissimilar materials *J. Appl. Phys.* **108** 044914
[13] Zhang P, Lau Y Y and Gilgenbach R M 2011 Thin film contact resistance with dissimilar materials *J. Appl. Phys.* **109** 124910
[14] Zhang P, Lau Y Y and Gilgenbach R M 2010 Minimization of thin film contact resistance *Appl. Phys. Lett.* **97** 204103
[15] Zhang P, Lau Y Y and Timsit R S 2012 On the spreading resistance of thin-film contacts *IEEE Trans. Electron Devices* **59** 1936
[16] Zhang P 2012 *Doctoral Dissertation* University of Michigan-Ann Arbor
[17] See http://www.ansoft.com for MAXWELL software
[18] Hall P M 1967 Resistance calculations for thin film patterns *Thin Solid Films* **1** 277
[19] Allen L H, Zhang M Y, Mayer J W, Colgan E G and Young R 1991 Solutions to current crowding in circular vias for contact resistance measurements *J. Appl. Phys.* **70** 253